3678 *Chem. Mater.* **2010,** *22,* 3678–3692
DOI:10.1021/cm100422z

CHEMISTRY OF MATERIALS
Article

Chevrel Phases, $M_xMo_6T_8$ (M = Metals, T = S, Se, Te) as a Structural Chameleon: Changes in the Rhombohedral Framework and Triclinic Distortion

Elena Levi* and Doron Aurbach

Department of Chemistry, Bar-Ilan University, Ramat-Gan, Israel 52900

Received February 10, 2010. Revised Manuscript Received May 13, 2010

It is commonly accepted that the nature of triclinic distortion, responsible for the superconductivity loss in Chevrel phases, is different for the two main structural types: electronic instability of the Mo_6-cluster in the compounds with large cations (type I) and "freezing" of the formerly mobile small cations in fixed positions (type II). Recently, for Chevrel phases with small cations, we proposed an alternative mechanism of the phase transition as one of the ways to attain the steric matching between the cations and the framework. It was shown that the triclinic structure is more flexible than the rhombohedral because it allows for additional deformations and a relative tilt of the main structural elements. Bond valence analysis performed for the first time for a variety of Chevrel phases in this work shows that the intrinsic instability of the binary compounds, Mo_6T_8, does not arise from the Mo_6-cluster anisotropy, but rather from the extremely non-uniform distribution of the anion charge in their crystal structure. This distribution changes drastically with cation insertion or partial chalcogen-halogen substitution, resulting in compound stabilization. However, a steric mismatching between big cations such as Pb, Sr, or Ba and the framework of the large and rigid Mo_6T_8 blocks strongly destabilizes the structure. The mismatching is evident from the unreasonably high bond valence sums for these cations; it increases with the cation size. Triclinic distortion, occurring on cooling, is associated with minor atomic displacements, and consequently, only with partial relaxation of the bond strains. In contrast, application of pressure decreases fundamentally the constraints in the M−T bonding and prevents the material from the phase transition. Thus, this work presents a general mechanism of structural instability for all Chevrel phases and explains changes in the Mo_6-cluster shape in the framework of simple bond valence relations.

Introduction

Chevrel phases, $M^{n+}{}_xMo_6T_8$ (M = metal, T = S, Se, Te), first reported by Chevrel et al. in 1971,[1] are noteworthy for good thermoelectric[2] and catalytic[3] properties, but most interestingly, for their remarkable superconductivity associated with relatively high critical magnetic fields ($T_c \approx 15$ K and $H \approx 60$ T for $PbMo_6S_8$), two phenomena which are normally mutually exclusive.[4−7] Because of this unusual combination, Chevrel phases are regarded as possible candidates for high-field superconducting magnets.[7] Recent interest in these materials is also related to the unique mobility of various mono- and divalent cations in the sulfides and selenides at ambient temperatures.[8−13] Owing to their high electronic and ionic conductivity, the sulfides and selenides can be used as cathodes in "green" rechargeable Mg batteries,[14,15] or as ceramic membranes for selective cation extraction from liquid wastes.[16] On the basis of a full bond valence analysis, performed for the first time for the Chevrel phase family, this work offers a new explanation for important structural features such as the structural instability and its relation to the Mo_6-cluster anisotropy.

The crystal structure of Chevrel phases (space groups $R\bar{3}$ or $P\bar{1}$) can be described as a framework of quasi-rigid

*To whom correspondence should be addressed. E-mail: elenal@mail.biu.ac.il.

(1) Chevrel, R.; Sergent, M.; Prigent, J. *J. Solid State Chem.* **1971**, *8*, 515.
(2) Caillat, T.; Fleurial, J.-P.; Snyder, G. *J. Solid State Sci.* **1999**, *1*, 535.
(3) Afanasiev, P.; Bezverkhyy, I. *Appl. Catal., A* **2007**, *322*, 129.
(4) Yvon, K. In *Current Topics in Material Science*; Kaldis, E., Ed.; Elsevier: North-Holland, Amsterdam, 1979; Vol. *3*.
(5) *Topics in Current Physics: Superconductivity in Ternary Compounds I*; Fisher., Ø., Maple., M. B., Eds.; Springer-Verlag: Berlin, 1982.
(6) Pena, O.; Sergent, M. *Prog. Solid State Chem.* **1989**, *19*, 165.
(7) Hampshire, D. P. In *Handbook of Superconducting Materials*; Cardwell, D., Ginley, D. S., Eds.; IOP: Bristol, U.K., 2002; Vol. *2*.
(8) Schollhorn, R. In *Inclusion Compounds*; Atwood, J. L., Ed.; Academic Press: London, 1984; Vol. *1*.
(9) Tarascon, J. M.; Hull, G. W.; Marsh, P.; Haar, T. *J. Solid State Chem.* **1987**, *66*, 204.
(10) Gocke, E.; Schramm, W.; Dolscheid, P.; Schollhorn, R. *J. Solid State Chem.* **1987**, *70*, 71.
(11) Levi, E.; Gershinsky, G.; Aurbach, D.; Isnard, O.; Ceder, G. *Chem. Mater.* **2009**, *21*, 1390.
(12) Levi, E.; Gershinsky, G.; Aurbach, D.; Isnard, O. *Inorg. Chem.* **2009**, *48*, 8751.
(13) Levi, E.; Mitelman, A.; Aurbach, D.; Brunelli, M. *Chem. Mater.* **2007**, *19*, 5131 (and references inside) .
(14) Aurbach, D.; Lu, Z.; Schechter, A.; Gofer, Y.; Gizbar, H.; Turgeman, R.; Cohen, Y.; Moskovich, M.; Levi, E. *Nature* **2000**, *407*, 724.
(15) Levi, E.; Gofer, Y.; Aurbach, D. *Chem. Mater.* **2010**, *22*, 860.
(16) Seghir, S.; Boulanger, C.; Diliberto, S.; Lecuire, J.-M.; Potel, M.; Merdrignac-Conanec, O. *Electrochem. Commun.* **2008**, *10*, 1505.

 Published on Web 05/26/2010

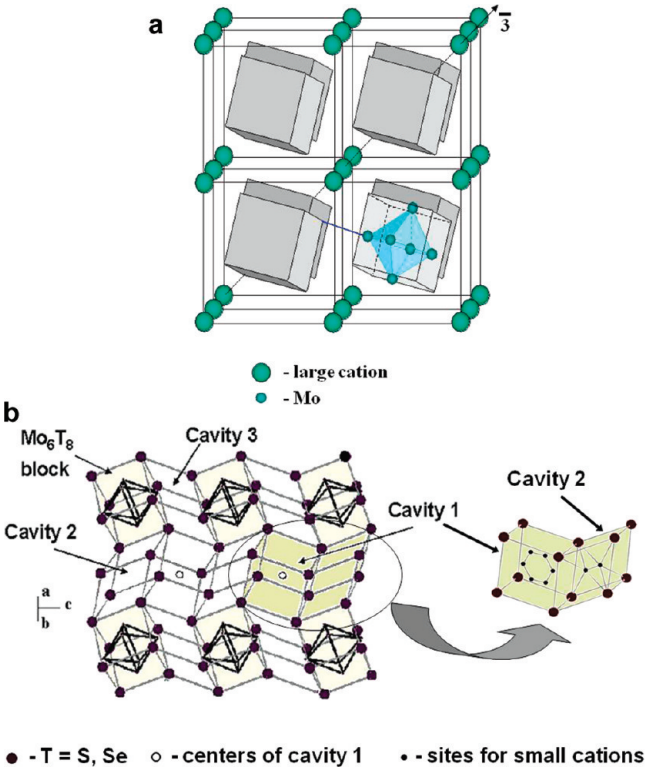

Figure 1. Crystal structure of Chevrel phases. (a) Type I with large cation in the origin (eight rhombohedral unit cells): Each cation is surrounded by eight Mo_6T_8 blocks. The internal structure is shown for one of the blocks. Intercluster Mo−T_1 bond is marked by blue. (b) Three type of pseudo-cubic cavities between the Mo_6T_8 blocks. Cavities 1 and 2 form the diffusion channels in three directions (A channel in one of the directions is shown here). Sites for small cations in cavities 1 and 2 are presented separately on the right.

Mo_6T_8 blocks or Mo_6-octahedral clusters inside anion cubes (Figure 1a).[4,5] Additional Mo−Mo and Mo−T bonds link the blocks into a three-dimensional network. The blocks form a system of open three-dimensional channels (Figure 1b), while the Mo_6-clusters preserve exceptionally local electroneutrality: Each Mo_6-cluster can easily accept up to four electrons. Thus, the crystal structure seems to be perfectly convenient for cation insertion. However, a question arises: How does the framework formed by the large and rigid Mo_6T_8 blocks remain stable upon insertion of such a wide variety of cations (about 40), ranging in chemical character and size?

One of the ways of the cation adjustment to the framework was discovered by Yvon[4] who showed that large (> 1 Å) cations, such as Pb, Sn, Ag, and La, are located at (or very close to) the origin of cavity 1, while small (< 1 Å) cations, such as Cu, Ni, Co, and Fe, are shifted away from the origin, forming six (equivalent for $R\bar{3}$) sites in cavity 1 (Typically the shift is normal to the $\bar{3}$ symmetry axis). Consequently, a classification into two structural types was proposed:[4−6] type I, Chevrel phases with large cations and $x = 1$, and type II, Chevrel phases with small cations. In the latter case, the cations with commonly tetrahedral anion environment can be distributed among cavities 1 and 2, resulting in $x \leq 4$. Moreover, Yvon suggested[4] that a spontaneous cation motion between

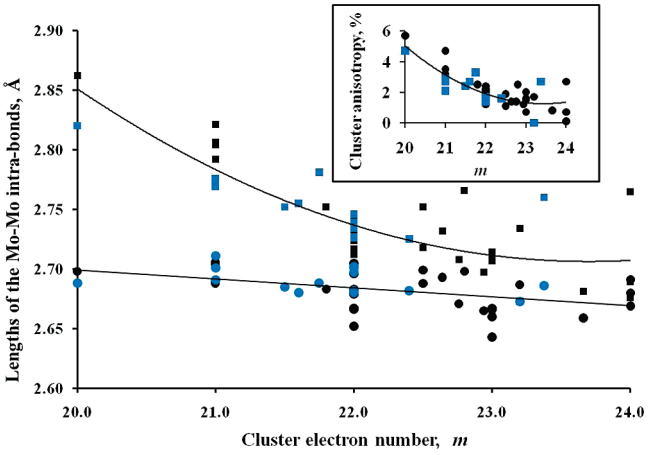

Figure 2. Lengths of the Mo−Mo intracluster bonds and their relative difference or the Mo_6-cluster anisotropy (in the inset) versus the cluster electron number. The data related to the sulfides and selenides are marked in black and blue, respectively.

the equivalent, closely located sites in cavity 1 is possible even at room temperature. In this way, small cations may occupy larger effective volume than big cations. To emphasize the unusual character of the cation shift, he introduced the term of cation "delocalization", as well as showed its correlations with rhombohedral angle and importance for structure characterization.[4]

Yvon was also the first who demonstrated the effect of the cation charge on the shape of the Mo_6-cluster.[4] In general, this shape is anisotropic: The bonds normal to the $\bar{3}$ symmetry axis are shorter than others. This anisotropy was initially explained by an electronic effect,[17] but later Corbett[18] assigned it to a steric conflict between strong Mo−T intercluster bonding and closed-shell anion repulsion ("matrix effect"). Figure 2 presents the variations in the Mo−Mo distances (and the Mo_6-cluster anisotropy as a relative difference between the long and the short Mo−Mo intracluster distances) versus the cluster electron number. The latter can be expressed as a sum of 20 electrons[4] (the total electron number in the Mo_6-cluster of the hosts, Mo_6T_8) and nx: $m = 20 + nx$, where $nx \leq 4$. As can be seen, the Mo_6-cluster distortion is maximal in the binaries, Mo_6T_8, and decreases with cation insertion, while the most symmetric, regular Mo_6-octahedra can be found in fully intercalated compounds $M^{n+}{}_xMo_6T_8$ with $nx = 4$.

According to Yvon,[4] the Mo−Mo interactions inside the Mo_6-cluster are covalent, with stronger and more symmetric bonding for larger electron number. Thus, the Mo_6-cluster contraction upon cation insertion was explained by the electron (charge) transfer from the cation to the Mo_6-cluster and even to the selenium anion, resulting in different cluster electron number: 20 for Mo_6S_8, 21 for Mo_6Se_8, and more than 22 for Mo_6Te_8.[4] Consequently, the maximal intercalation level was predicted to be equal to 4 and 3 electrons per Mo_6-cluster for the sulfides and selenides, respectively. However, subsequent electrochemical studies[8−10] clearly showed that, for

(17) Anderson, O. K.; Klose, W.; Nohl, H. *Phys. Rev. B* **1978**, *17*, 1209.
(18) Corbett, J. D. *J. Solid State Chem.* **1981**, *37*, 335.*39*, 56.

both the sulfide and selenides, insertion is possible for up to $nx = 4$. The idea of the charge transfer effect on the cluster shape was criticized by Corbett,[18] who demonstrated that the Mo−Mo bond contraction inside the Mo_6-cluster is compensated by elongation of the Mo−Mo bonds between the Mo_6-clusters.

According to Corbett, cation insertion is associated with "loosening" of the Mo−T bonds between the blocks (interbonds), which, in turn, results in smaller distortion of the Mo_6-cluster. Corbett[18] was the first who used the Pauling strengths (which are the basis of the modern bond valence model) to compare the metal−metal interactions within the Mo_6-clusters for Chevrel phases and similar compounds. He showed that, in spite of the unusual case (metal−metal bonding), the bond strength relations are applicable and useful for the structure rationalization. However, at that time, elaboration of the bond valence model was only in its infancy, so that important structural features remained beyond the scope of his considerations. Thus, some ambiguity still remains concerning the nature of the Mo_6-cluster anisotropy and its changes with cation insertion.

Moreover, it is commonly accepted to correlate the Mo_6-cluster shape to the material stability.[4−6] The latter has two aspects. The first is the high-temperature instability of the sulfide host, Mo_6S_8, which can be obtained only at ambient temperatures by chemical or electrochemical removal (leaching) of ternary metal (Cu, Ni, etc.) from stable compounds such as $Cu_{1.8}Mo_6S_8$ or $Ni_2Mo_6S_8$.[4,5,8] In contrast, the selenide and telluride binaries, as well as most of the materials with ternary metals, $M^{n+}{}_xMo_6T_8$, are thermally stable. The sulfide-based Chevrel phases can also be stabilized by partial sulfur substitution for halogens with formation of compounds such as $Mo_6S_6Br_2$ and $Mo_6S_6I_2$.[4,5] According to Yvon,[4] the material stability increases with the cluster electron number, that is, the compounds with $m = 24$ should be the most stable. However, the synthetic studies seem to be in contradiction with this statement: For such cations as Li^+, Na^+, Mg^{2+}, Cd^{2+}, and so forth, it is relatively simple to obtain the Chevrel phases with $nx = 1$ or 2 by the direct high temperature synthesis, but compounds with $nx = 4$ can be prepared only by chemical or electrochemical cation insertion into the Mo_6T_8 (T = S, Se) hosts at ambient temperatures.[12] Thus, the reason for the completely different thermal stability of Chevrel phases, as well as its relation to the Mo_6-cluster anisotropy remains unclear.

The second aspect is the transition from rhombohedral ($R\bar{3}$) to triclinic ($P\bar{1}$) phase.[4−6] Normally triclinic distortion in Chevrel phases is associated with minor atomic displacements, as strong intercluster interactions (see the Mo−T bond marked in blue in Figure 1) protect the structure from significant changes. The phase transition is affected by pressure, temperature, and composition. At ambient conditions, the Mo_6T_8 hosts and most of the $M_xMo_6T_8$ compounds are rhombohedral,[4−6] while triclinic crystals are more typical for compounds with small cations, especially selenides.[19−21] It was shown[6] that superconducting properties, usual for type I, are absent for triclinic crystals, but they may be restored in the same material by applying high pressure, which inhibits the phase transition.

According to Yvon,[4,22] the origin of the triclinic distortion is different for the two main structural types: electronic (or magnetic) instability of the Mo_6-clusters for type I and "freezing" of the formerly mobile small cations in fixed positions for type II. It was also mentioned[22] that the Mo_6T_8 units change their relative orientation during triclinic distortion, thus evoking cation ordering at low temperature. However, this idea of changes in the linkage of the Mo_6T_8 units was not illustrated or advanced. Moreover, the origin of the phase transition remained unclear: In general, "frozen cations, which lost their mobility, can be distributed randomly between the same six equivalent sites, maintaining rhombohedral symmetry. Similarly, mobile cations may occupy only two equivalent positions in cavity 1, resulting in triclinic symmetry. Our studies[11,12] revealed that the cation mobility in Chevrel phases is rather independent on the crystal symmetry. For instance, Mg^{2+} ion transport at ambient temperature is faster in the triclinic selenide than in the rhombohedral sulfide.

Recently, we proposed an alternative mechanism: The triclinic distortion in Chevrel phases was regarded as one of the ways to attain the steric matching between the cations and the framework.[23] It was shown that the triclinic structure is more flexible than the rhombohedral one because it allows additional deformations of cavity 1 and the Mo_6T_8 blocks, as well as their relative tilt (Figure 3). As a result, it can better ensure relaxation of the steric constraints that may occur on cooling. For instance, the phase transitions in $Cu_xMo_6S_8$ ($x \geq 1.8$), $Fe_2Mo_6S_8$, and $MgMo_6Se_8$ allow retaining the Cu−Cu and Fe−Fe pairs in the low-temperature forms or result in more symmetric environment around cations (Change in the coordination number of Fe^{2+} and Mg^{2+} ions from 4 to 5). The study[23] was devoted mainly to compounds of type II, but the Table in Figure 3 illustrates that the mechanism of the triclinic distortion, namely, the tilt of the main structural units, is the same for all Chevrel phases. Thus, it is logical to suggest that the origin of the phase transition is also the same, and this is a relaxation of the bond strains caused by steric mismatching.

To verify this suggestion, we have to revise the structural changes in Chevrel phases related to cation insertion. In spite of intensive studies in the past, full bond valence analysis has never been applied to this material family. Ignoring the bond valence relations resulted in the unlikely oxidation state of 0.7 for Ni or artificial ideas about the formation of polynuclear complexes, such as

(19) Roche, C.; Chevrel, R.; Jenny, A.; Pecheur, P.; Scherrer, H.; Scherrer, S. *Phys. Rev. B* **1999**, *60*, 16442.
(20) Belin, S.; Chevrel, R.; Sergent, M. *J. Solid State Chem.* **2000**, *155*, 250.
(21) Mancour-Billah, A.; Chevrel, R. *J. Solid State Chem.* **2003**, *170*, 281.
(22) Yvon, K. *Solid State Commun.* **1978**, *25*, 327.
(23) Levi, E.; Mitelman, A.; Aurbach, D.; Isnard, O. *Inorg. Chem.* **2007**, *46*, 7528.

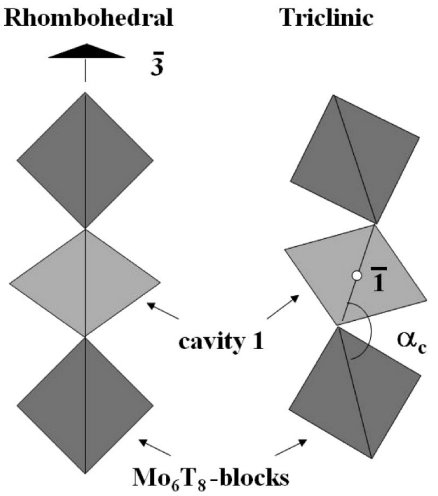

CPs	Temperature, K	Tilt angle α_c, deg
$EuMo_6S_8$	40	178.0
$BaMo_6S_8$	173	178.4
$Cu_{1.8}Mo_6S_8$	250	178.1
$Fe_2Mo_6S_8$	300	173.9
$Cr_{1.7}Mo_6S_8$	300	173.9
$MgMo_6Se_8$	300	176.1
$Ti_{0.9}Mo_6Se_8$	300	173.8
$Ni_{0.7}Mo_6Se_8$	300	176.9
$FeMo_6Se_8$	300	176.4

Figure 3. Schematic relative arrangement of the main structural elements in the rhombohedral and triclinic Chevrel phases structures. The table presents the tilting angle α_c between the diagonals of pseudocubic cavity 1 and the Mo_6T_8-blocks lying on the $\bar{3}$ symmetry axis in rhombohedral crystals.

$(Zn_2)^{2+}$, $(Cd_2)^{2+}$, $(Li_4)^{3+}$, $(Ni_3)^{2+}$, and $(Ni_2)^{2+}$ in the crystal structure of these compounds.[8,20,24]

Thus, the aim of this paper is to perform the bond valence analysis for a variety of Chevrel phases to clarify the origin of the structural instability, as well as their possible relation with Mo_6-cluster distortion. Special attention will be devoted to the effect of cation insertion, temperature, and pressure on the structural changes in these materials.

Bond Valence Method

Bond valence calculations are based on the empirical correlation between the bond valence S_{ij} and the its length R_{ij}:[25−27]

$$S_{ij} = \exp[(R_0 - R_{ij})/0.37] \quad (1)$$

where R_0 is the tabulated[25] bond valence parameter for "cation−anion" pairs.

These calculations become routine in structure analysis field: If a crystal structure determination is correct, the bond valence sum (BVS) of any atom calculated according to the experimental interatomic distances R_{ij} should be equal to the expected value of its oxidation state V (or to the total number of bonding electrons):

$$\sum S_{ij} = V \quad (2)$$

Thus, BVS calculations allow one (i) to confirm the reliability of the crystal structure solution; (ii) to find the coordination number (CN) and the oxidation state of cations based on the bond lengths (examples of such determinations for Chevrel phases are presented in the Supporting Information); and (iii) to refine the cation positions in the crystal structures using soft distance constraints (in this case, we have to know the cation oxidation state. See section SIV in the Supporting Information). On the basis of the BVS values, we can also choose the sites with the appropriate geometry for ionic transport.[28] In our previous work on Chevrel phases, we demonstrated the effectiveness of the BVS method for crystal structure determination, and diffusion analysis.[11−13,29] In this paper it was used to characterize bond strains and their effect on the structural instability of these compounds.

As it is clear from eqs 1 and 2, non-stressed bonding can be described by a regular, non-distorted coordination polyhedron with identical bond lengths, R_{ij}, which can be defined as R_{ideal}:

$$R_{\text{ideal}} = R_0 - 0.37 \ln(V/\text{CN}) \quad (3)$$

To characterize the lattice-induced strains, Brown in his book,[27] devoted to the bond valence model, proposed to use two parameters. The first is the bond strain index (BSI):

$$\text{BSI} = \langle (S - s)^2 \rangle^{1/2} \quad (4)$$

where S is the experimental bond valence calculated from the observed bond length and s is the theoretical bond valence, equal to V/CN. The angle brackets $\langle\ \rangle$ indicate an average taken over all the bonds in the formula unit. If the value of the BSI for a particular crystal is greater than 0.05 vu, the structure can be regarded as strained.

The second measure of lattice strain is the global instability index (GII):

$$\text{GII} = \left\langle \left(\sum S_{ij} - V_i \right)^2 \right\rangle^{1/2} \quad (5)$$

Here, the average is taken over all the atoms in the formula unit. The difference $\sum S_{ij} - V_i$ is also known as a discrepancy factor. This index sets the extent to which the

(24) Prigge, C.; Muller-Warmuth, W.; Gocke, E.; Schollhorn, R. *Solid State Ionics* **1993**, *62*, 143.
(25) Brese, N. E.; O'Keefee, M. *Acta Crystallogr.* **1991**, *B47*, 192.
(26) Brown, I. D. *Acta Crystallogr.* **1992**, *B48*, 553.
(27) Brown, I. D. *The chemical bond in inorganic chemistry: the bond valence model*; Oxford University Press: New York, 2006.
(28) Adams, S.; Swenson, J. *Phys. Rev. B* **2000**, *63*, 54201. Adams, S.; Swenson, J. *J. Phys.: Condens. Matter* **2005**, *17*, S87.
(29) Levi, E.; Mitelman, A.; Isnard, O.; Brunelli, M.; Aurbach, D. *Inorg. Chem.* **2008**, *47*, 1975.

valence sum is violated. A structure with GII < 0.05 vu can be defined as non-strained, while GII values greater than about 0.20 vu should be associated with unstable material.

As can be seen, both the indexes, BSI and GII, are related to the entire crystal structure. To follow the structural changes caused, for instance, by insertion of different cations into Mo_6T_8, it is important to show the bond strains in separate coordination polyhedra. Thus, in addition to the global indexes, we used similar, but local parameters, which, by analogy with internal stresses in the composite materials, were defined as uniform and non-uniform bond strains. The latter characterizes a distortion of coordination polyhedra, which was calculated as a standard deviation of the experimentally determined bond lengths (R_{ij}) or valences (S_{ij}) from their average value. For instance, it is known from the structural data[4] that the environment of the Cu^+ cation in $Cu_{1.8}Mo_6S_8$ is a distorted tetrahedron with Cu−S bonds of 2.319, 2.345, 2.381, and 2.457 Å, and respective valences of 0.289, 0.269, 0.245, and 0.199 vu (The tabulated[25] bond valence parameter R_0 of Cu−S bonds, equal to 1.86 Å, and eq 1 were used to calculate the valence values). As can be seen, the BVS is equal to 1.00 vu, that is, to the formal oxidation state of Cu^+. Thus, the non-uniform strain of the Cu−S bonds, expressed as a standard deviation of S_{ij}, is equal to 3.9%.

In the case of bonds under uniform strain, the use of tabulated bond valence parameters R_0 results in BVS values, which are clearly different from V. To obtain the correct V value, it is necessary to introduce a new value of the bond valence parameter, R_0', which differs from the tabulated R_0. Hence, the uniform strain can be defined as a relative difference between R_0' and R_0 (or BVS and V, if we use R_0). The new R_0' can be calculated directly from the structural data, using eqs 1 and 2 (see examples in the Supporting Information). Note that such calculation is possible for any atom, if we know its coordination number, the lengths of its bonds, as well as its oxidation state (or the number of bonding electrons).

For instance, according to the structural data,[30] the environment of Ba^{2+} ion in $BaMo_6S_8$ is a distorted cube with two Ba−S(2) bonds of 2.968 Å and six Ba−S(1) bonds of 3.209 Å. On the basis of the tabulated[25] R_0 value of 2.77 Å, BVS = $2 \times 0.586 + 6 \times 0.305 = 3.00$ vu. To obtain a BVS value equal to the formal oxidation state of Ba^{2+}, it is necessary to decrease the bond valence parameter to 2.62 Å. This means that the coordination polyhedron around Ba is not only distorted, but also severely condensed. The distortion and the shortening of the Ba−S bonds can be defined as the non-uniform and uniform components in the bond stressing, respectively. The uniform strain was calculated to be $100 \times (R_0' - R_0)/R_0 = -5.4\%$ or $100 \times (V - \mathrm{BVS})/V = -50\%$ (the strain related to compression is commonly accepted to be negative).

To determine the R_0' for the Mo−Mo bonds, we used the same procedure. Each Mo atom is connected to five Mo atoms (four bonds within individual Mo_6-cluster and an additional bond between neighboring clusters), with bond lengths, R_{ij}, which can be found from the atomic coordinates. Thus, we can use five eqs 1, which correlate the unknown bond valence strengths, S_{ij}, with the known R_{ij}. In addition, according to eq 2, the sum $\sum S_{ij}$ for the five bonds should be equal to the Mo electron number, $m/6$. By solving these six equations, we can easily determine the six unknowns, S_1, S_2, S_3, S_4, S_5, and R_0'.

To analyze the Mo−T bonding in Chevrel phases, we calculated the bond valence parameters R_0' for the Mo(cluster)−T pairs. Mo atoms are located approximately in the centers of the Mo_6T_8 block faces (Figure 1a). Thus, each Mo atom is coordinated by four anions of the same face (three T_1 and single T_2) and by additional T_1 anion from adjacent block. Similar to other R_0', the R_0' parameters of the Mo(cluster)−T bonds can be found for any $M^{n+}{}_xMo_6T_8$ with known crystal structure and known values of n and x, by using eqs 1 and 2, the lengths of the five Mo−T bonds, R_{ij}, and the formal oxidation state of Mo, V (the details of such calculations can be found in the Supporting Information).

In conclusion, it is important to emphasize the basic difference in the application of the tabulated bond valence parameters, R_0, and R_0', calculated in this work for each compound in accordance with its structural data. Without R_0, we cannot compare the real strained structure with the unstrained one; thereby the knowledge of the tabulated parameters is crucial in calculation of the uniform bond strains or the global instability indexes. In contrast, we cannot use R_0 to determine the valence input of different bonds in the strained structure, for instance, to calculate the extremely non-uniform charge of T_1 and T_2 anions, or to verify the charge balance in the crystal structure. For this, it is necessary to use R_0', which are individual for each compound.

Results and Discussion

Steric Adjustment of the Mo_6T_8 Framework to Cation Size: Main Features. *Deformation of Cavity 1 As a Function of the Cation Size*. In the previous work,[23] we have shown that the main structural changes upon cation insertion occur in cavity 1 (see Figure S1 in the Supporting Information). As a result of the strong intercluster bonding, variation in the edges of the pseudocubic cavity 1 for different cations does not exceed ~8% (e.g., the shortest S_1-S_1 bond changes from 3.337 Å for Mo_6S_8 to 3.645 Å for $BaMo_6S_8$), while the increase in the cation size may reach 200% (compare the radii of Li^+ and Ba^{2+} ions of 0.68 and 1.38 Å, respectively). Hence, the steric matching in rhombohedral Chevrel phases is attained by various contractions of the cavity along the $\bar{3}$ symmetry axis, accompanied by a cation displacement from the origin (Figure 4). The contraction can be expressed as the relative difference between the short and the long diagonals of the pseudocube (distances $T_2 - T_2$ and $T_1 - T_1$ in Figures 4a and b, respectively). Tabulated bond valence parameter R_0 can be used to characterize the cation size (see Figure S2 in the Supporting Information), but R_0 does not take into account the cation oxidation state (V)

(30) Kubel, F.; Yvon, K. *Acta Crystallogr.* **1987**, *C43*, 1655.

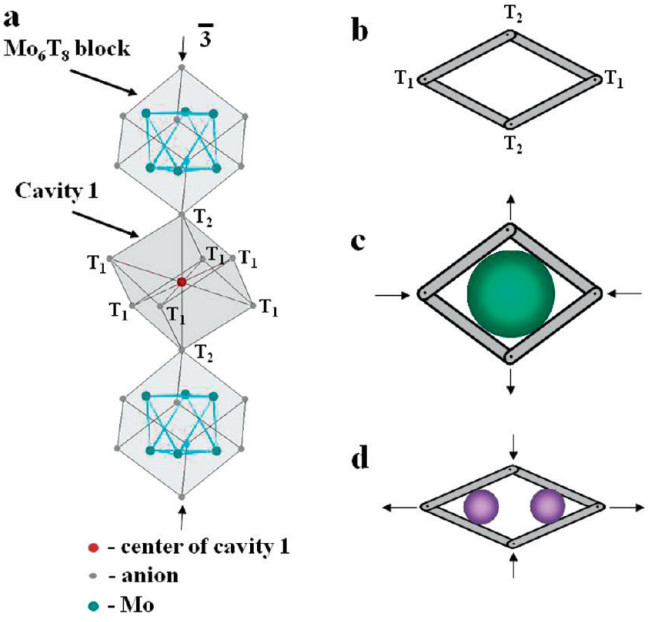

Figure 4. (a) Alternation of pseudocubic cavities 1 and the Mo_6T_8 blocks along $\overline{3}$ symmetry axis. (b, c, d) Schematic cross-section of cavity 1 for Mo_6T_8 (b), type I with large cation (c), type II with small, shifted cation (d). The arrows show the compression and extension forces.

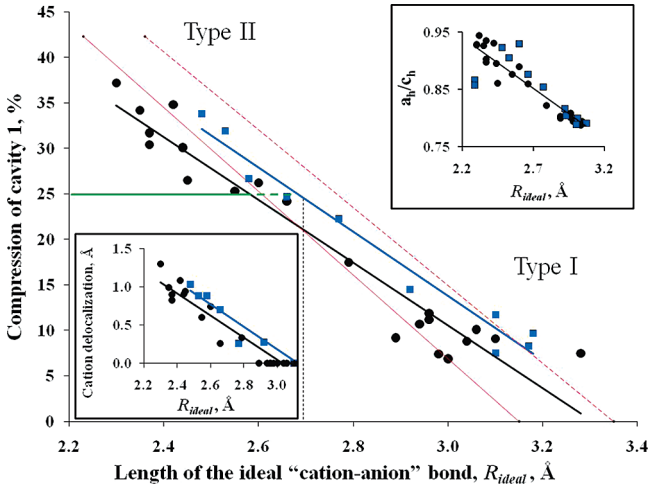

Figure 5. Compression of cavity 1 (relative difference between long and short diagonals of pseudocube in percent) and cation delocalization (in the lower inset) as functions of the ideal "cation−anion" bonds (bond length in a regular coordination polyhedron). The data related to the sulfides (circles) and selenides (squares) are marked by black and blue, respectively. Red solid and dashed lines (for the sulfides and selenides, respectively) present a linear approximation between regular cubic and tetrahedral coordination. The green solid and dashed lines show the squeezing of cavity 1 in pure Mo_6S_8 and Mo_6Se_8, respectively. The upper inset shows the ratio between the hexagonal unit cell parameters as a function of the ideal "cation−anion" bonds.

and its coordination number (CN). Thus, in our previous work[12,23] we proposed to use the lengths of the ideal "cation−anion" bond, R_{ideal}.

Figure 5 illustrates the effect of the cation size (R_{ideal}) on the compression of cavity 1 along the $\overline{3}$ axis and cation delocalization (in the lower inset) (see also Table S1 in the Supporting Information. Structural data for the Chevrel phases can be found in refs 4−6,12,13,23,30−35). As expected, the larger the cation, the smaller the contraction of cavity 1 along the axis and the cation delocalization. The cavity deformation is clearly different for the two main structural types.[4,5] Actually, in the binary compounds, Mo_6T_8, the compression is 25%. In Chevrel phases with large cations (radius >1 Å) it changes from 22 to 24% for Ag^+ to 7% for La^{3+}, while in Chevrel phases with small cations (radius <1 Å) it can reach values as high as 37% (for Ni^{2+}). However, the type definition for the Na^+ or Ag^+-containing compounds is rather problematic: According to the structural data,[4,12] these cations may remain in the origin of cavity 1, forming bonds only with two T_2 anions, or they may be displaced toward tetrahedral coordination.

Interestingly, the compression value can be roughly predicted by linear interpolation between two boundary cases (red lines in Figure 5): It is minimal and equal to zero for a regular anion cube, and maximal and equal to 42.3% when the two axial T_2 anions are in contact. In the latter case, the shortest diagonal of the cube is equal to its edges, that is, cavity 1 is formed by six regular tetrahedra. The critical cation radii, corresponding to these two boundary cases, can be calculated using the ionic radii of sulfur and selenium (1.82 and 1.93 Å, respectively) and the first Pauling rule: The critical ratio between cation and anion radii in stable structures is equal to 0.732 and 0.225 for cubic and tetrahedral environments, respectively. According to this simple model, for the same cation, the cavity contraction for the selenides should be higher than for the sulfides, but in practice this difference is relatively small, probably because of the higher flexibility of the more polarizable selenium framework.

In spite of the clear general correlation, evident from Figure 5, one can see that the compression of cavity 1 is almost the same for all large cations, with maximal deviation from the red "prediction" line for the biggest cations. The unexpectedly high values of the cavity contraction for large cations such as Pb, Sr, or Ba seem to show that the simple deformation mechanism of steric matching between the Mo_6T_8 framework and the cation size is not sufficiently effective for them. This conclusion will be verified later with the bond valence analysis.

Deformations of the Entire Mo_6T_8 Block in Rhombohedral Chevrel Phases. These deformations are much less pronounced than those of cavity 1, but they are also affected mainly by the size of the inserted cations (see Figure S1 in the Supporting Information).[23] Decrease in the cation size is accompanied by elongation of the Mo_6T_8 block along the $\overline{3}$ axis, which partially compensates the respective contraction of cavity 1 in this direction. Nevertheless, the decisive effect of cavity 1 on the framework dimensions results in a quasi-linear correlation between the ratio of the hexagonal unit cell parameters, a_h/c_h, and the ideal "cation−anion" bond lengths, R_{ideal} (see the upper inset in Figure 5).

(31) Kubel, F.; Yvon, K. *J. Solid State Chem.* **1988**, *73*, 188.
(32) Jorgensen, J. D.; Hinks, D. G.; Noakes, D. R.; Viccaro, P. J.; Shenoy, G. K. *Phys. Rev. B* **1983**, *27*, 1465.
(33) Ritter, C.; Gocke, E.; Fischer, C.; Schollhorn, R. *Mater. Res. Bull.* **1992**, *27*, 1217.
(34) Levi, E.; Lancry, E.; Mitelman, A.; Aurbach, D.; Ceder, G.; Morgan, D.; Isnard, O. *Chem. Mater.* **2006**, *18*, 5492.
(35) Le Berre, F.; Pena, O.; Perrin, C.; Padiou, J.; Horyn, R.; Wojakowski, A. *J. Alloys Compd.* **1998**, *280*, 85.

Bond Valence Relations in the Mo_6T_8 Blocks and Cavity

1. *Compensation Mechanism and the Mo_6-Cluster Anisotropy*. The shape of the Mo_6-cluster may be regular in two cases: (i) a completely symmetric anion and cation environment around the Mo_6-cluster, or (ii) the sum of atomic forces, resulting from the asymmetric environment and affecting the Mo_6-cluster normal to all their faces, should be equal to zero. Such regular Mo_6-cluster, with the Mo−Mo bond of 2.700 Å, was found, for instance, in cubic $K_7[Mo_6Se_8(CN)_6]\cdot 10H_2O$, where each Mo atom is bonded to the CN group.[36] In the crystal structure of Chevrel phases, the Mo_6-cluster environment is always asymmetric because of a different bonding of T_1 and T_2 anions (see below). The anisotropic cluster shape testifies that the atomic forces along the $\bar{3}$ symmetry axis are not identical to those normal to the axis. In this case the lengths of the Mo−Mo intrabonds follow another compensation mechanism: For each Mo atom, the strengths of the four intracluster Mo−Mo bonds have to compensate the strengths of the five Mo−T bonds and the single Mo−Mo intercluster bond. This compensation mechanism can be expressed mathematically, on the basis of the following considerations: First, the valence sum of the five Mo−Mo bonds for each Mo atom should be equal to the number of its electrons, which assist in the intra- and intercluster bonding (so-called[4] VEC):

$$\sum S_{Mo\text{-}Mo} = m/6 \tag{6}$$

Second, the valence sum for the five Mo−T bonds for each Mo atom should be equal to its formal oxidation state, V:

$$\sum S_{Mo(c)\text{-}T} = V \tag{7}$$

In addition, $m/6$ can be found[4,18] as the difference between the number of valence electrons (six for Mo) and the formal oxidation state, V: $m/6 = 6 - V$ or

$$\sum S_{Mo\text{-}Mo} = 6 - \sum S_{Mo(c)\text{-}T} \tag{8}$$

Thus, the BVS of the Mo−Mo bonding is directly related to the BVS of the Mo−T bonding. For instance, for the hosts, Mo_6T_8 ($m = 20$), $\sum S_{Mo(c)-T} = 2^2/_3$, that is, $\sum S_{Mo-Mo} = 6 - 2^2/_3 = 3^1/_3$.

To illustrate this correlation, it is useful to consider a hypothetical regular Mo_6-cluster with identical Mo−T bonds and the Mo−Mo intercluster bond equal to the intracluster bonds (Figure 6a). In this case, for Mo_6S_8, $s_{Mo(c)-T} = 0.533$ and $s_{Mo-Mo} = 0.667$. In the real structure (Figures 6b−e), the intercluster Mo−Mo bond is always longer than the intracluster bonds because of the framework geometry. In addition, the five Mo−T bonds, as well as the angles between the inter- and intrabonds are also different. As a result, in general, any combinations of the Mo−Mo intrabonds, which are adequate for the block geometry and obey eq 8, are possible, that is, the bond distortion in the Mo_6-cluster has to be a normal phenomenon.

Effect of Inserted Cations on the Mo−Mo and Mo−T Bonding. Figures 7a and 7b show respectively the bond valence parameters of the Mo−Mo and Mo (cluster)−T bonds, calculated for a wide variety of Chevrel phases (31 sulfides and 15 selenides), as a function of the cluster electron number, m (For details, see Section SII, Tables S2 and S3 in the Supporting Information. Structural data for these calculations can be found in ref 4−6,12,13,19,20,23,29−35,37). As can be seen, $R_0{}'_{Mo-Mo}$ are independent of m, confirming the Corbett's conclusion:[18] The contraction of the Mo−Mo intracluster bonds is compensated by elongation of the Mo−Mo intercluster bonds. The absolute values of the $R_0{}'_{Mo(c)-T}$ parameters also agree with the Corbett's statement on the unusually strong Mo−T interactions in Chevrel phases. In fact, these values are fundamentally lower than the tabulated ones (2.35 Å for the Mo−S bonds and 2.49 Å for the Mo−Se pair), but similar by other characteristic features: The $R_{0\ Mo(c)-T}$ for the selenides are essentially larger than those for the sulfides. Moreover, their ratio, $R_{0\ Mo(c)-Se}/R_{0\ Mo(c)-S}$, found from the graph (e.g., 2.31/2.18 = 1.060 for $m = 22$) is very close to that of the tabulated bond valence parameters for the Mo−Se and Mo−S pairs, $R_{0\ Mo-Se}/R_{0\ Mo-S}$ (2.49/2.35 = 1.060).

However, the changes in the Mo−T bonding caused by cation insertion are more complicated than those described by Corbett. As can be seen from Figure 7b, in spite of the relatively high scattering, $R_0{}'_{Mo(c)-T}$ clearly decrease with m, and this decrease is very similar for the sulfide and the selenides. Thus, the higher the cluster electron number, the stronger are the Mo_6-cluster interactions with the anion environment. It means that the compression of the Mo−T intrabonds for the larger m exceeds the stretching of the Mo−T interbond, which may arise from cation insertion. It should be mentioned that the effect of the cluster electron number on the Mo−T bonding results in the obvious distinction of the introduced $R_{0\ Mo(c)-T}$ (which can be found from the linear correlations in Figure 7b) from usual bond valence parameters. The latter are normally constant for each "cation−anion" pair; they are independent of the ion charge. In contrast, $R_{0\ Mo(c)-T}$ are a-priory related to the total charge of the inserted cations, nx. In fact, $R_{0\ Mo(cluster)-T}$ should be constant only for compounds with the same m. In spite of this limitation, the introduced parameter is very useful for understanding bonding in Chevrel phases.

For instance, on the basis of the obtained values of $R_{0\ Mo-Mo}$ and $R_{0\ Mo(c)-T}$, it can be shown (see Figures S3 and S4 in the Supporting Information) that the distortion of the Mo−Mo and especially the Mo−T bonds increases with larger cation size. Moreover, all the bonds adjust themselves to the cation size: The Mo−Mo bonds are slightly stretched in the compounds with small cations and compressed in Chevrel phases with large cations. This

(36) Mironov, Y. V.; Virovets, A. V.; Naumov, N. G.; Ikorskii, V. N.; Fedorov, V. E. *Chem.—Eur. J.* **2000**, *6*, 1361.

(37) Cava, R. J.; Santoro, A.; Tarascon, J. M. *J. Solid State Chem.* **1984**, *54*, 193.

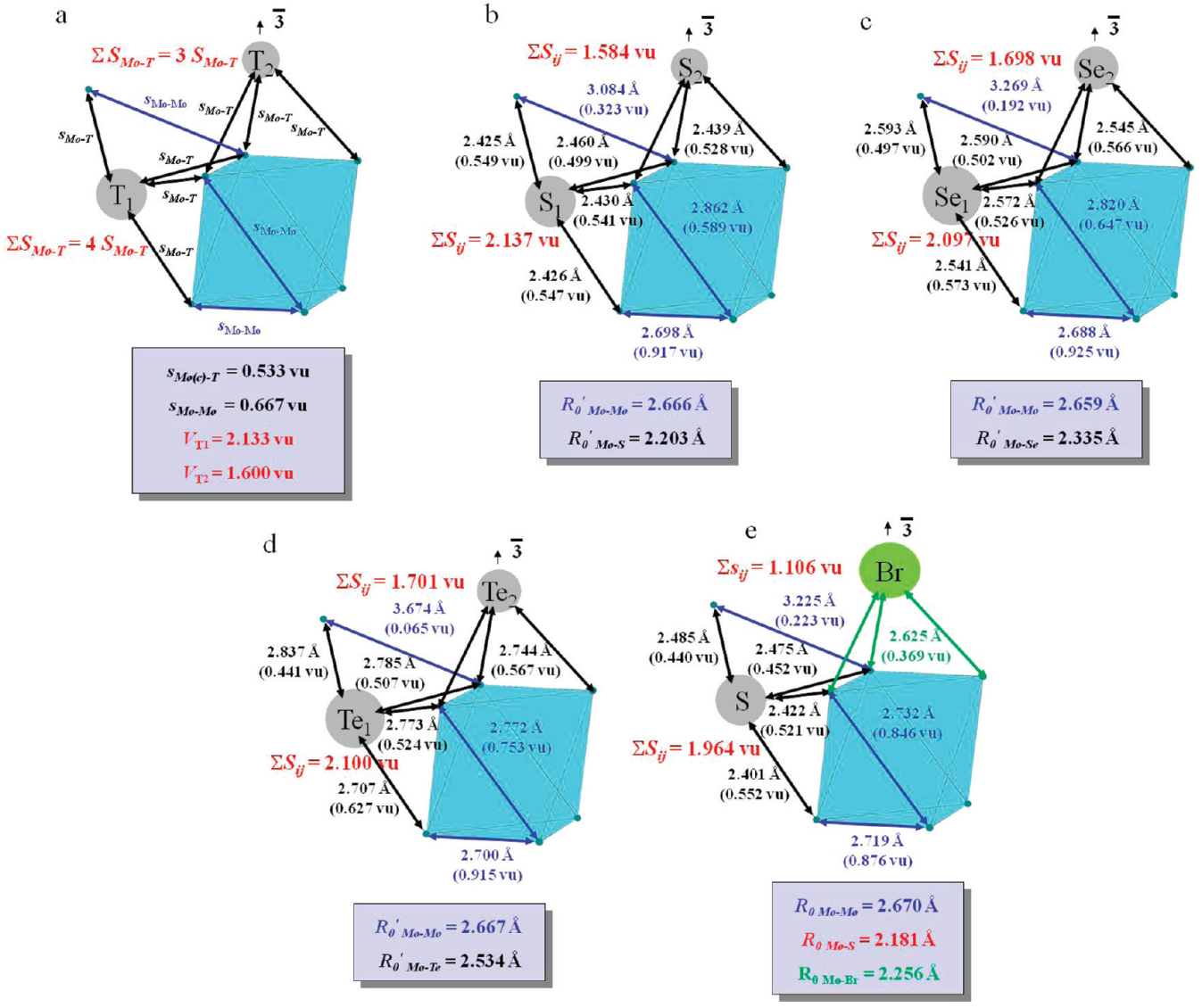

Figure 6. Bond valence relations in the crystal structure of the binaries: (a) hypothetic case of a regular Mo_6-cluster with identical Mo−Mo and Mo−T bonds; (b) Mo_6S_8; (c) Mo_6Se_8; (d) Mo_6Te_8; (e) $Mo_6S_6Br_2$.

effect is compensated by a slight elongation of the Mo−T bonds with insertion of larger cations. These correlations are more obvious for the sulfides than for the selenides.

Non-Uniform Anion Charge and Instability of the Binaries. Calculations based on the structural data allow determination not only the $R_0'_{Mo-Mo}$ and $R_0'_{Mo(c)-T}$ parameters, but also the valence of each bond, S_{ij}. Thus, Figure 6, in addition to the bond lengths in the Mo_6T_8 blocks of the hosts, shows also their valences. Interesting detail is the absence of the Mo−Mo intercluster bonding in Mo_6Te_8 (Figure 6d): The respective valence is lower than the accepted[18,28] limit of 0.075 vu. The ratio $R_0'_{Mo(c)-Te}/R_0'_{Mo(c)-Se} = 2.534/2.335 = 1.085$ for the binaries is close to that of the tabulated bond valence parameters for the Mo−Te and Mo−Se pairs, $R_{0\ Mo-Te}/R_{0\ Mo-Se}$ (2.69/2.49 = 1.080).

Using the valences, we can calculate the bond valence sum, $\sum S_{ij}$, for two structurally different anions, T_1 and T_2 (For details, see section SIII and Table S4 in the Supporting Information). The result of this elementary operation is crucial for structure rationalization: The valence distribution in the Mo_6T_8 crystal structure is extremely non-uniform, simply because of the environment difference around anions (Figures 6b−c): The T_2 anions located on the $\bar{3}$ symmetry axis are coordinated by **three** Mo atoms, and their bond valence sums are equal to 1.584, 1.698, and 1.701 vu for T_2 = S, Se, and Te, respectively. The bond valence sums of the T_1 anions (general position) bonded by **four** Mo atoms are 2.137, 2.097, and 2.100 vu for T_1 = S, Se, and Te, respectively. Note the important detail: The average valence of the eight anions, $2T_2 + 6T_1$, per formula unit is very close to their formal oxidation state: 1.999, 1.997, and 2.000 vu for T = S, Se, and Te, respectively, which confirms the relevance of such calculations.

To clarify the origin of the striking difference between the bond valence sum and the formal oxidation state of T^{2-} anion, let us assume that this difference is caused by strains in the Mo(c)−T bonds. Equation 1 can be rewritten:

$$0.37 \ln(V/\mathrm{CN}) = R_0 - R_{ij} \qquad (9)$$

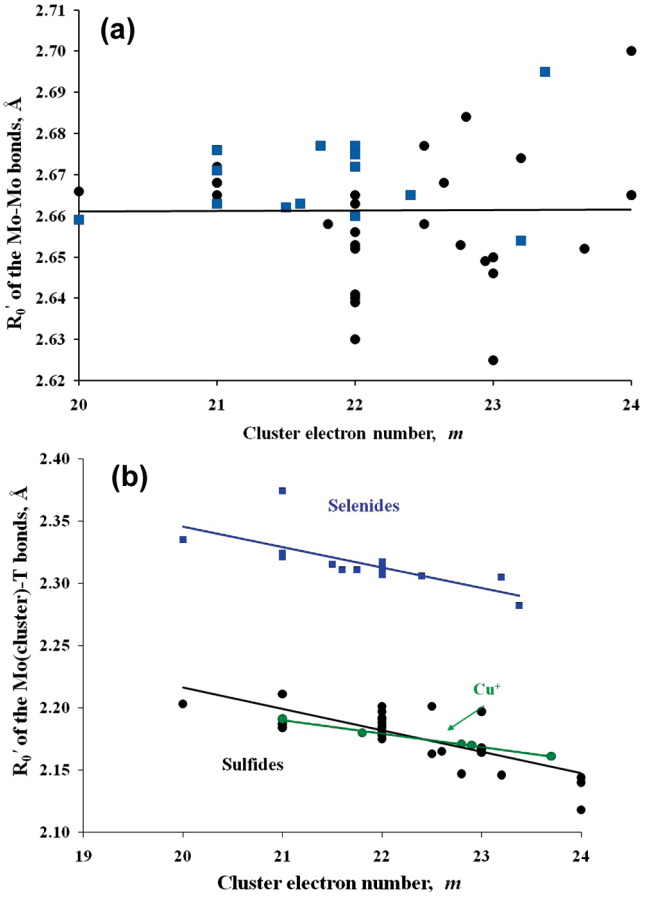

Figure 7. Bond valence parameters R_0' of the Mo−Mo (a) and the Mo(cluster)−T (b) bonds as a function of the cluster electron number. The data related to the sulfides (circles) and selenides (squares) are marked by black and blue, respectively. The green line corresponds to $Cu_xMo_6S_8$.

All three Mo(c)−T_2 bonds are identical because of the crystal symmetry (rhombohedral). Their length can be defined as R_2. Thus, for the T_2 anion:

$$0.37 \ln(2/3) = R_0 - R_2 \quad (10)$$

The four Mo(c)−T_1 bonds are not the same, but their average value can be defined as R_1. Hence, for the T_1 anion:

$$0.37 \ln(2/4) = R_0 - R_1 \quad (11)$$

From here, the difference $(R_1 - R_2) = 0.1$ Å, that is, to reach the matching anion valence, the average value of the Mo(c)−T_1 bond lengths should be fundamentally higher than the length of the Mo(c)−T_2 bonds. As can be seen from Figure 6, this is not the case: the lengths of the M−T_1 and Mo−T_2 bonds are close. Thus, the violated valences indicate the real change in the anion charge, which is so unusual for S^{2-} and Se^{2-} anions, that is, we can speak not only about difference in the valence sums, but also about strikingly non-uniform anion charge in the crystal structure of Chevrel phases.

For more profound understanding of the intimate relationships between the Mo−T bond lengths (which, in turns, are related to the Mo−Mo bond lengths) and the

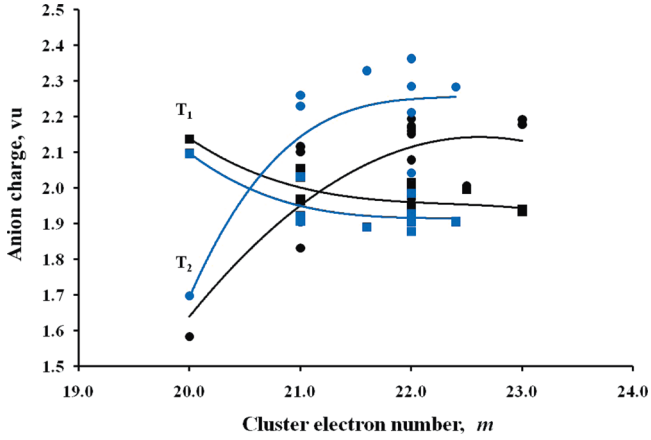

Figure 8. Redistribution of the anion charge with cation insertion. The data related to the sulfides and selenides are marked by black and blue, respectively.

valence sum of T_1 and T_2 anions, it seems useful to come back to the hypothetical "idealized" crystal structure presented in Figure 6a. Taking into account the number of the anion bonds and their equivalent input in the anion charge ($V_{T1} = 4s_{Mo-T}$ and $V_{T2} = 3s_{Mo-T}$), it is clear that $V_{T1} = 2.133$ vu and $V_{T2} = 1.600$ vu. Note that the local electroneutrality in the structure is retained:

$$6V_{T1} + 2V_{T2} = 8 \times 2 \text{ vu} \quad (12)$$

Thus, even in the "idealized" structure, the bond valence sum of the two anions differs fundamentally because of the difference in their coordination, that is, the Mo_6-cluster environment is a priori asymmetric.

Because of the distortion of the [MoT_5] polyhedra and different input of inserted cations into the anion charge, a symmetric Mo_6-cluster may be related to another ratio between valence sums of the T_1 and T_2 anions. A nice illustration is the crystal structure of $Mo_6S_6Br_2$ (m = 22 vu, crystal data can be found in ref 5), in which the S_2 anions are substituted by Br (Figure 6e). The Mo-(cluster)−Br bonds noticeably weaker than the Mo-(cluster)−S bonds: $R_{0\ Mo(c)-T}$ are equal to 2.256 and 2.181 Å, respectively, with their ratio of 1.034 (Note that the ratio of the tabulated parameters for the Mo−Br and Mo−S pairs is the same: 2.43/2.35 = 1.034). As a result, a relatively symmetric Mo_6-cluster exists in this compound, where the bond valence sums are equal to 1.106 vu for Br (T_2) and 1.964 vu for sulfur (T_1).

Using eq 5, we calculated the global instability index (GII), which is equal to 0.20 vu for Mo_6S_8, 0.15 vu for Mo_6Se_8, 0.13 vu for Mo_6Te_8, and 0.05 vu for $Mo_6S_6Br_2$. As can be seen, these results agree well with our knowledge about different stability of these compounds (see the Introduction). Note the important detail: 93−95% of the GII is related to the violated valence of T_1 and T_2 anions. In fact, if we do not take into account the strains in the bonds around the Mo atom, the GII remains almost the same: 0.19 vu for Mo_6S_8 and 0.14 vu for Mo_6Se_8. Thus, the intrinsic instability of the binaries arises rather from the extremely non-uniform distribution of the anion charge in their crystal structure, but not from the Mo_6-cluster anisotropy.

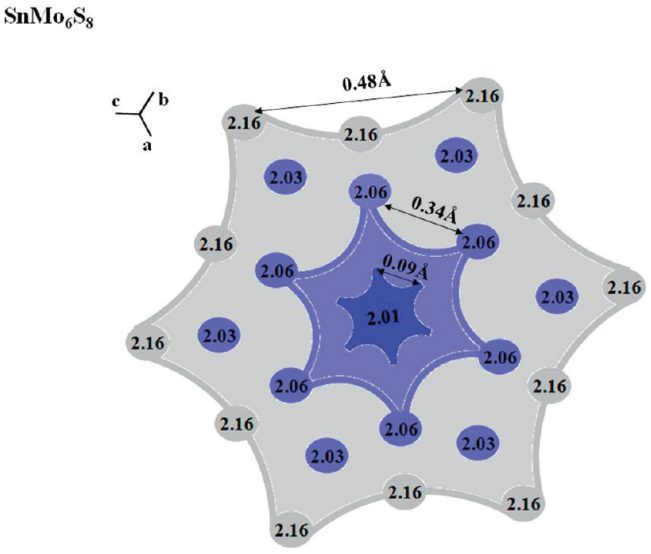

Figure 9. BVS maps of cavity 1 for $SnMo_6S_8$. The area with matching valence are marked by dark blue, the regions with 2 < BVS < 2.06 and 2.06 < BVS < 2.16 are colored by light blue and light gray, respectively.

Effect of Inserted Cations on the Charge of T_1 and T_2 Anions. In general, cation insertion always leads to bond valence redistribution in the crystal structure of intercalation compounds, while a larger input into the anion charge is related to more charged cations. For Chevrel phases, the bond valence rearrangement results in drastic changes in the anion charge distribution (Figure 8; see also Table S4 in the Supporting Information): It remains non-uniform (the exception is the sulfides with $m \approx 21$ vu and selenides with $m \approx 20.5$ vu), but for the compounds with single cation in cavity 1, the negative charge excess is typical for T_2 anions (Note that the cation location in cavity 2 may change these relations). Thus, according to the correlations of Figure 8, it can be expected that ternary Chevrel phases with $m \approx 21$ vu should be the most stable because their bond valence sum for T_1 and T_2 anions are close to their formal oxidation state. However, this prediction is not effective because the ternary phases' stability is greatly affected by the bond strains in the cation polyhedra.

Bond Strains in the Cation Polyhedra. It is clear that for a proper bond valence analysis, it is crucial to know the exact atomic positions in the unit cell. For Chevrel phases, it is commonly accepted[4,32] that large cations are not located exactly in the origin of cavity 1, but slightly "delocalized". The cation shift was estimated by anisotropy of the thermal vibrations, which are obviously higher in the plane normal to the $\bar{3}$ symmetry axis than along the axis. Alternatively, we can correlate the cation location to the minimum on the valence maps.[27,28] This method was found to be useful for Chevrel phases with small cations,[11−13,29] because their tetrahedral (or similar) environment is associated with clear point minimum on the BVS maps, which corresponds to the tetrahedron center. However, the same maps for the large cations in the plane normal to the $\bar{3}$ symmetry axis (Figure 9. The method of the valence mapping is presented in section SIV of Supporting Information) revealed an important detail: Instead of a point minimum, such map

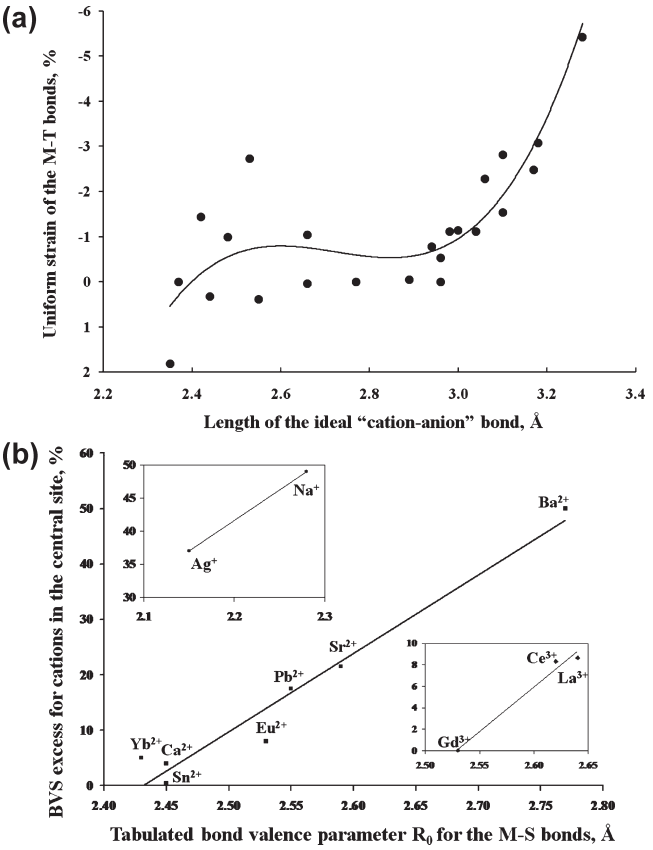

Figure 10. (a) Uniform strain (compression) of the M−T bonds in Chevrel phases as a function of the ideal "cation−anion" bond. (b) BVS excess (relative difference between bond valence sum and formal oxidation state in percent) for a number of divalent cations in the central site as a function of their bond valence parameter R_0 in the sulfides. The insets show the same correlation for monovalent and trivalent cations.

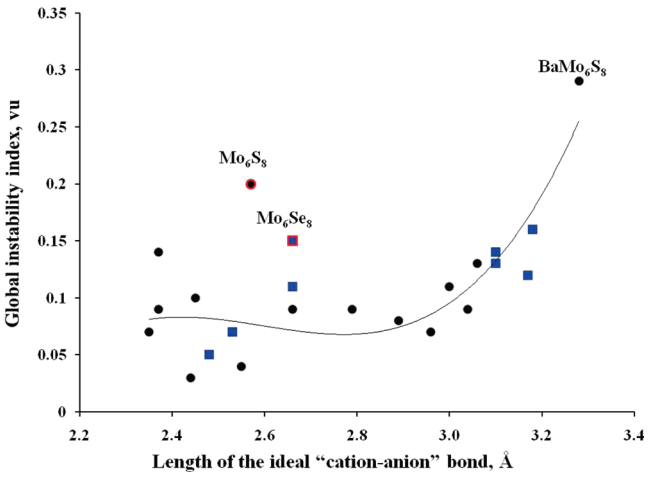

Figure 11. Global instability index of Chevrel phases as a function of the ideal "cation−anion" bond.

shows a relatively large area with the same BVS value, that is, variations in the atomic position inside this area do not affect the cation−anion bonding. Existence of such area explains the origin of the high and anisotropic thermal vibrations of the large cations in Chevrel phases. Moreover, for such broad BVS minimum, the only criterion of choice for cation location is a minimal potential energy of the cation site. For Chevrel phases, this is the origin of cavity 1

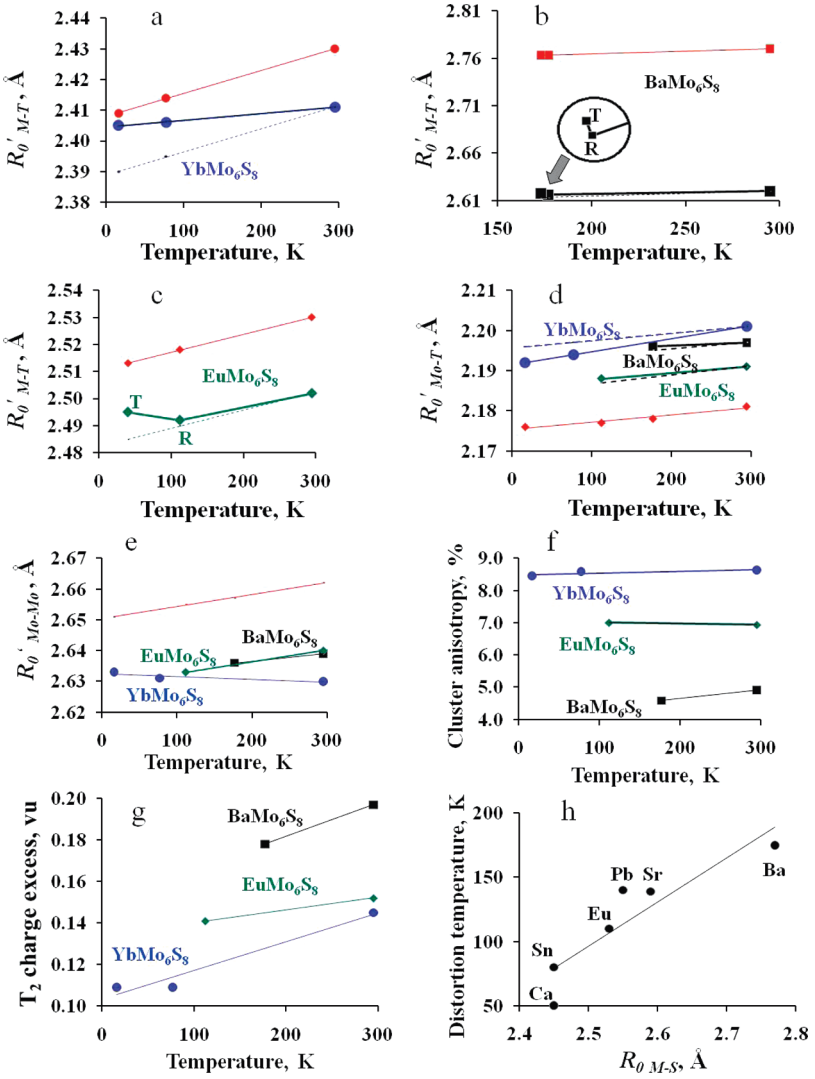

Figure 12. (a−g) Effect of temperature on the structural characteristics of $YbMo_6S_8$, $BaMo_6S_8$, and $EuMo_6S_8$: bond valence parameters R_0' of the M−T (a, b, c), Mo−T (d), and Mo−Mo (e) bonds; Mo_6-cluster anisotropy (f) and T_2 excessive charge (g). (h) Temperature of triclinic distortion in MMo_6S_8 (M = Ca, Sn, Eu, Pb, Sr, and Ba) versus tabulated bond valence parameter for the M−S bonds. The red lines in panels a−e present the "theoretical" drop of tabulated R_0 caused by cooling. The dotted lines show the decrease in the R_0' predicted by the theory. Rhombohedral and triclinic symmetry of the phases is marked by R and T, respectively.

with minimal "cation-Mo" repulsion. Thus, it seems reasonable to suggest that large cations are located exactly in the origin of cavity 1.

It can be shown (see Figure S6 in the Supporting Information) that the non-uniform strain or the distortion of the cation polyhedra (expressed as a standard deviation of the bond valences, S_{ij}, from their average value) is high for almost all Chevrel phases, and it is independent of the cation size. The reason is the rigid cubic shape of the Mo_6T_8 blocks, which predetermines the distorted cation environment. In contrast, the uniform strain, presented as a relative difference between R_0' and R_0 of the M−T bonds in Figure 10a, is clearly different for two structural types: For the major part of the compounds with "small" cations (type II, CN = 4), the uniform strain is relatively low and independent of their sizes, while for the type I (CN = 8), it increases drastically for larger cations. The compression of the M−T bonds is compensated by stretching of the anion−anion bonds in cavity 1. For instance, for $BaMo_6S_8$, the distances between sulfur atoms, which form the cavity, are equal to 3.631 and 3.645 Å, instead of the reference value of 3.35 Å proposed for these compounds by Corbett.[18]

As was mentioned above, the uniform strain results in the excessive bond valence sums calculated with tabulated R_0. In fact, Figure 10b (see also Table S5 in the Supporting Information) presents the BVS excess (the relative difference between the BVS and V, (BVS − V)/V, in percent) for a number of divalent cations in the central site as a function of their bond valence parameter R_0. The insets show the same correlation for the mono- and trivalent cations. The larger the cation, the higher its BVS excess for the central site, and the higher is the abnormal shortening of the "cation−anion" bonds as compared to similar bonds in non-strained sulfides and selenides. Thus, cavity I is not really convenient for such large cations as Pb, Sr, or Ba. As a result, the global instability index (GII), which is essentially lower for most of the ternary phases as compared to the binaries, increases systematically for the large cations

Table 1. Bond Valence Relations for Sn^{2+} Cation in the $SnMo_6S_8$ at Ambient Pressure

	lattice parameters, Å							
Chevrel phases	a_h	c_h	bonds	bond number	length, Å	$R_0'_{Sn-S}$, Å	bond valence, vu	bond valence sum, vu
$SnMo_6S_8$ ref 4	9.174	11.377	Sn−S_1	6	3.083	2.450	0.181	
			Sn−S_2	2	2.738		0.459	2.00
$SnMo_6S_8$ ref 35	9.180	11.375	Sn−S_1	6	3.089	2.423	0.165	
			Sn−S_2	2	2.677		0.504	2.00

and reaches the value of 0.29 vu for $BaMo_6S_8$ (Figure 11. For details, see Table S6 in the Supporting Information). For the latter, 97% of GII is related to the strain in the cation polyhedron. Such high values of the instability index agree with the fact that hot-pressing (pressure of 0.17−0.3 GPa at 1400 °C) is needed to stabilize the Chevrel phases with these cations upon their synthesis.[6]

Effect of Temperature on the Bonding in the Cation Polyhedra. Brown[27] gives a simple formula for the calculation of bond valence parameters at different temperatures:

$$R_0{}^T = R_0 + (\mathrm{d}R/\mathrm{d}T)\Delta T \qquad (13)$$

where $\mathrm{d}R/\mathrm{d}T$ is a thermal expansion of the bond, which can be found based on the exponential correlation between $\mathrm{d}R/\mathrm{d}T$ and the bond valence (see Figure S7 in the Supporting Information): The weaker the bond, the more pronounced is its change with cooling. Thus, eq 13 allows predicting the decrease in the bond length on cooling in the structure without uniform strain. Alternatively, we can calculate the R_0' values for any compound (with strained and non-strained bonds) directly from the structural data obtained at different temperatures (for details, see Table S7 in the Supporting Information). A comparison between predicted, "theoretical" and "experimental" bond valence parameters may provide information on the bond strains.

It should be emphasized that in the range from 0 to 295 K, structural changes in the Chevrel phase' bonding caused by cooling is rather delicate (Figures 12a−g). Thus, for proper comparison, we used only high quality structural data, obtained for the same samples at different temperatures.[30,32,38] For all three compounds, $BaMo_6S_8$, $EuMo_6S_8$, and $YbMo_6S_8$, the contraction of the M−T and Mo−Mo bonds is smaller than the predicted one, that is, cooling results in a slight strain relaxation in these bonds (Figures 12a−c and e). The relaxation in the M−T bonds becomes more pronounced in the first two compounds after their triclinic distortion (Figures 12b and c). The stretching of the Mo−T bonds is smaller than the predicted one in $YbMo_6S_8$, but higher in $BaMo_6S_8$ and $EuMo_6S_8$ (Figure 12d). Variations in the Mo_6-cluster anisotropy are minor, it even decreases slightly with cooling in $YbMo_6S_8$ and $BaMo_6S_8$ (Figure 12f). The anion charge becomes more uniform with cooling (Figure 12g).

It is clear that instability of Chevrel phases with large cations does not change drastically on cooling, even after the phase transition (For details, see Table S8 in the Supporting Information). Thus, a direct driving force of the triclinic distortion in $BaMo_6S_8$ and $EuMo_6S_8$ is not

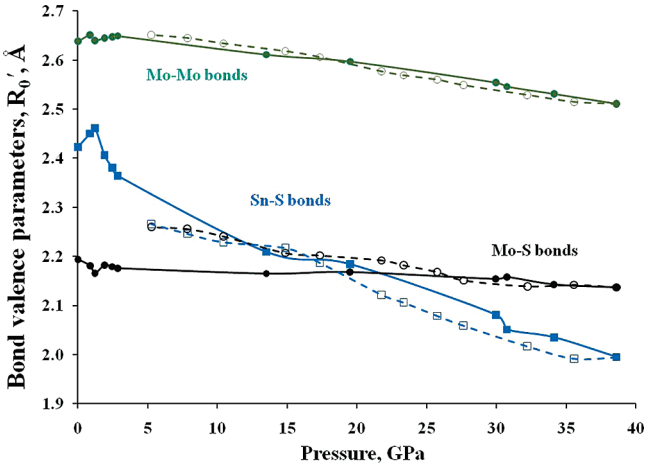

Figure 13. Effect of pressure on the bond valence parameters R_0' of the Mo−Mo, Mo−S, and Sn−S bonds in $SnMo_6S_8$.

obvious (maybe this is the additional stretching of the Mo−T bonds). However, a relatively good correlation between the cation size (expressed as the bond valence parameter, $R_{0\ M-S}$) and the phase transition temperature (Figure 12h), rather ignored in the previous works,[4−7,38−40] seems to be meaningful because this is the excessive cation size, which is responsible on the high material instability for this type of Chevrel phases (it should be mentioned that there is an essential difference in distortion temperature presented in different studies, for example, for $PbMo_6S_8$ and $CaMo_6S_8$,[6,39,40] that is, this temperature is very sensitive to conditions of material preparation).

Structural Changes at High Pressure. In the earlier works,[6,7] it was found that application of pressure inhibits the structural transformation in Chevrel phases. For instance, $EuMo_6S_8$ at pressure above 7 kbar retains its rhombohedral symmetry at low temperatures, showing superconductivity with Tc up to 11 K. Recently Ehm et al.[41] studied in detail structural changes caused by pressure for $SnMo_6S_8$. It was shown that compression results in a gradual decrease in the rhombohedral lattice parameters, a_r and α_r, as well as in Mo_6-cluster distortion (preferential contraction normal to the $\bar{3}$ symmetry axis) and its rotation with respect to the unit cell edges.

The Mo_6-cluster distortion was explained[41] by changes in the Sn−S bonding: According to Ehm et al.[41] the Sn−S_1 bonds (3.08 Å), existing in the material at normal

(38) Kubel, F.; Yvon, K. *Acta Crystallogr.* **1990**, *C46*, 181.
(39) Johnson, D. C.; Tarascon, M.; Sienko, M. J. *Inorg. Chem.* **1985**, *24*, 2598.
(40) François, M.; Yvon, K.; Cattani, D.; Decroux, M.; Chevrel, R.; Sergent, M.; Boudjada, S.; Wroblewski, Th. *J. Appl. Phys.* **1994**, *75*, 423.
(41) Ehm, L.; Dera, P.; Knorr, K.; Winkler, B.; Krimmel, A.; Bouvier, P. *Phys. Rev. B* **2005**, *72*, 14113.

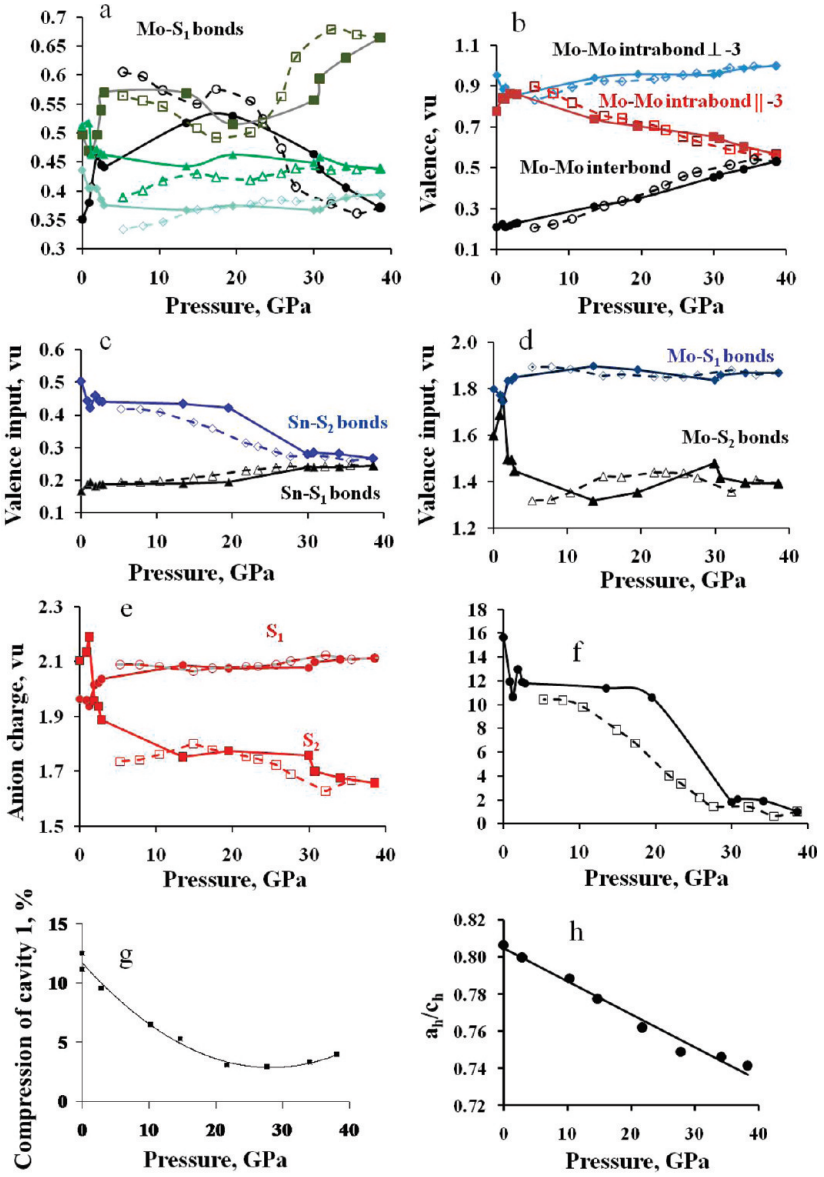

Figure 14. Effect of pressure on the structural parameters of $SnMo_6S_8$: valence of the individual Mo−S_1 (a) and Mo−Mo (b) bonds; valence contribution of the Sn−S (c) and Mo−S (d) bonds into the S_1 and S_2 anion charge; S_1 and S_2 anion charge (e); non-uniform strain (standard deviation of the bond valences in percent) of the Sn−S bonds (f); compression of cavity 1 (g) and ratio between unit cell parameters (h).

pressure, are too long and become effective only after their shortening at high pressure. However, bond valence calculations (Table 1), performed for $SnMo_6S_8$ according to eqs 1 and 2, and tabulated R_0 (2.45 Å) for Sn−S bonds, show that at normal pressure the input of the Sn−S_2 bonds into cation valence is only about 1 vu, that is, only a half of the Sn^{2+} charge. The input of the Sn−S_1 bond is higher than the accepted limit of 0.075 vu, that is, it cannot be ignored, and these bonds do contribute to the matching valence for the cubic site. Moreover, as we saw above, the effect of the M-cations on the Mo_6-cluster shape is related mainly to their charge, which remains constant in this experiment. Thus, the proposed mechanism for the structural changes under pressure seems to be inconvenient. In addition, it remained unclear how the structural changes caused by pressure could prevent the structure from triclinic distortion on cooling.

To clarify the mechanism, we have to look more carefully at the data. Figure 13 shows the variations in the bond valence parameters for $SnMo_6S_8$ as a function of pressure (the calculations assumed the constant oxidation state of Sn and Mo cations: +2 and $+2^1/_3$, respectively. For details, see Table S9 in the Supporting Information). Figure 14 presents the valence changes in the individual bonds and those in the anion charge input, as well as the compression of cavity 1, while Figure 15 (see also Figure S8 in the Supporting Information) illustrates the steric changes in the main structural elements. According to the bond theory,[42] a gradual shortening of all the bonds, especially the weaker ones, can be expected. However, the compression process is much more complicated; it should be divided into a number of steps, where contraction of some of the bonds is compensated by stretching of the others. For instance, when the pressure increases from ambient to 1.22 GPa, drastic contraction of the Mo−S_1 interbond,

(42) Brown, I. D.; Klages, P.; Skowron, A. *Acta Crystallogr., Sect. B* **2003**, *B59*, 439.

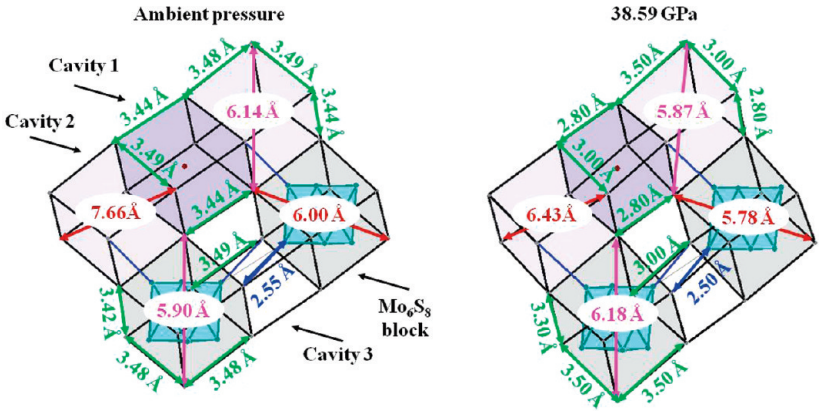

Figure 15. Steric changes, caused by high pressure, in the main structural elements of $SnMo_6S_8$.

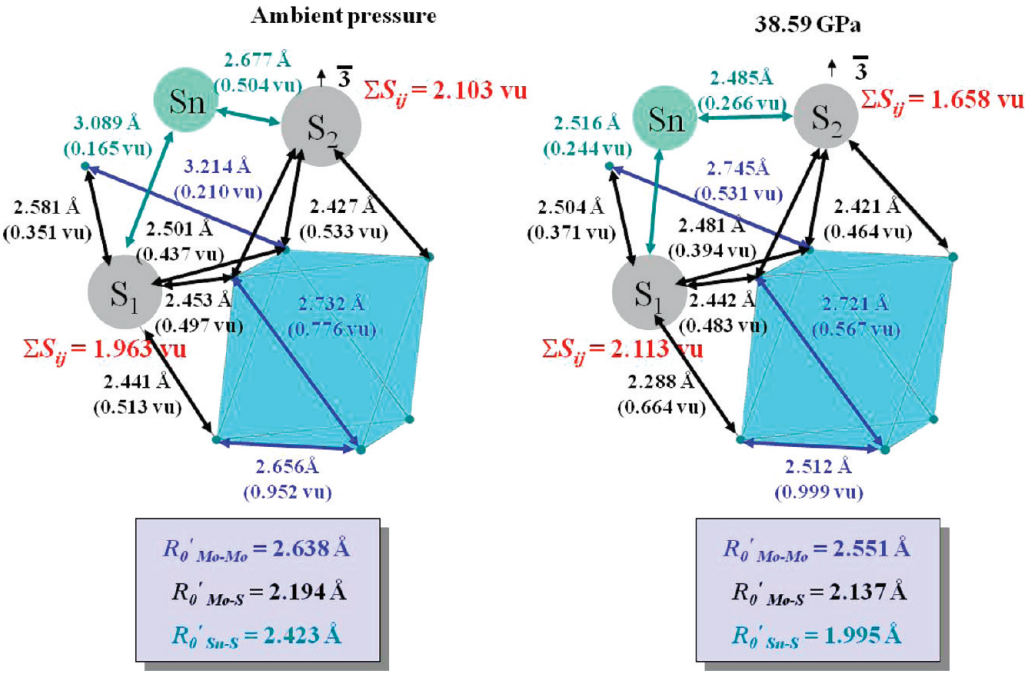

Figure 16. Bond valence relations in the crystal structure of $SnMo_6S_8$ at ambient and high (38.59 GPa) pressure.

the Mo−S_2 and Sn−S_1 bonds is compensated by stretching of the Sn−S_2 and Mo−S_1 intrabonds (Figures 14a,c,d). As a result, bond valence parameter R_0' of the Mo−S bonds slightly decreases, while R_0' of the Sn−S bonds clearly increases (Figure 13). The valence of the Mo−S_1 interbond reaches quickly (at 1.91 GPa) some critical values of 0.46 vu, typical for the intrabonds (Figure 14a).

After that, the compression mechanism changes: Slight elongation of the Mo−S_1 interbond is compensated by drastic shortening of one of the Mo−S_1 intrabonds in the range of 1.22−2.85 GPa (Figure 14a). In the range 2.85 to ~18 GPa, the Mo−S_1 interbond is compressed again, but the compression is more gradual. At higher pressure an opposite process of the loosening of the bond proceeds up to ~40 GPa (note that the Mo−Mo interbond strength continuously increases, Figure 14b). This loosening is compensated by shortening of the same Mo−S_1 intrabond (Figure 14a) with simultaneous contraction of cavity 3 along the rhombohedral axes, a_r (Figure 15). The strengths of the two other Mo−S_1 intrabonds (Figure 14a) and the Mo−S_2 bonds (Figure 14d) remain almost at the same, relatively low, level. Finally, the Mo−S_2 bonds are stretched, and the Mo−S_1 bonds are compressed (Figure 14d), resulting in the deficiency of the negative charge for the S_2 anion and its excess for the S_1 anion (Figure 14e). As the structure squeezing occurs mainly in the direction normal to the $\bar{3}$ symmetry axis (Figures 14h and 15), shortening of the Mo−Mo inter and intrabonds, quasi-parallel to this direction, is compensated by the weakness of the Mo−Mo bond along the symmetry axis (Figure 16).

As can be seen, the material response on the high pressure is not related to specific properties of Sn^{2+} cation, but rather to bonding in the Mo_6S_8 matrix. Thus, the results of ref 41 are very important because the effect found for $SnMo_6S_8$ should be similar for all Chevrel phases with large cations. It can be expected that their instability should increase with pressure because of the

higher violation of the T_1 and T_2 anion charge. However, in the previous sections it was shown that the instability for this type of Chevrel phases arises mostly from the lack of matching between the rigid rhombohedral framework and the excessively large cations. The results for $SnMo_6S_8$ demonstrate that this matching is better attained under high pressure. In fact, the essential loosening of the $Sn-S_2$ bonds (Figures 14c and 16), almost regular coordination polyhedron around Sn^{2+} cation (Figures 14f and 16), and smaller compression of cavity 1 with pressure (Figure 14g) testify that the latter should noticeably stabilize the MT_8 polyhedron, thus preventing the material from triclinic distortion.

Conclusions

Bond valence analysis performed in this work shows that the intrinsic instability of the binaries, Mo_6T_8 (T = S, Se, Te. The global instability index, GII, is equal to 0.20, 0.15, and 0.13 vu, respectively), arises rather from the extremely non-uniform distribution of the anion charge in their crystal structure, but not from the Mo_6-cluster anisotropy. This analysis illustrates also how insertion of relatively small cations or the T_2 anion substitution by halogen changes the bonding and stabilizes the materials (e.g., GII = 0.03 and 0.05 vu for $MgMo_6S_8$ and $Mo_6S_6Br_2$, respectively). In contrast, insertion of such large cations as Pb, Sr, or Ba, is associated with steric mismatching between the cations and the matrix, resulting in the high bond strains and structure destabilization (GII = 0.13, 0.14, and 0.29 vu for $PbMo_6S_8$, $SrMo_6S_8$, and $BaMo_6S_8$, respectively). The lattice strains are evident from the unreasonably high bond valence sums for these cations calculated with tabulated bond valence parameters, as well as from a relatively large compression of cavity 1 for the intercalation compounds (associated with extremely asymmetric MT_8-polyhedron).

Triclinic distortion in such compounds as $EuMo_6S_8$ and $BaMo_6S_8$ occurring on cooling, results in the minor atomic displacements, and consequently, only in a partial relaxation of the bond strains. In contrast, application of pressure leads to fundamental changes in bonding; in particular, to the more symmetric anion environment (bond valence analysis was performed for the data of ref 41 for $SnMo_6S_8$). As a result, high pressure should prevent the structure from large steric constraints in the cation environment and stabilize the Chevrel phases. We believe that this is the reason for the absence of triclinic distortion (and, respectively, for the appearance of superconductive properties) in the materials under high pressure.

Acknowledgment. We thank Prof. L. Ehm for supplying detailed information on the crystal structure of $SnMo_6S_8$ under high pressure.

Supporting Information Available: Additional data related to the bond valence analysis and structural changes in Chevrel phases caused by cation insertion, temperature, and high pressure. This material is available free of charge via the Internet at http://pubs.acs.org.